IET Radar 2022: International Conference on Radar Systems,
24-27 October 2022, Edinburgh, Scotland, UK
https://radar2022.theiet.org/

PERFORMANCE PREDICTION OF THE COHERENT RADAR DETECTOR ON MEASURED UAVS DATA

Massimo Rosamilia[1]* , Augusto Aubry[1], Alessio Balleri[2], Vincenzo Carotenuto[1], and Antonio De Maio[1]

[1]Department of Electrical Engineering and Information Technology, University of Naples "Federico II", Naples, Italy
[2]Centre for Electronic Warfare, Information and Cyber, Cranfield University, Defence Academy of the United Kingdom, Shrivenham, UK
**E-mail: massimo.rosamilia@unina.it*

Keywords: RADAR CROSS SECTION, MEASURED DATA, STATISTICAL ANALYSIS, RADAR DETECTION PERFORMANCE, DRONE DETECTION.

Abstract

This paper presents measurements of Radar Cross Section (RCS) of five Unmanned Aerial Vehicles (UAVs), comprising both consumer grade and professional small drones, collected in a semi-controlled environment as a function of azimuth aspect angle, polarization and frequency in the range 8.2-18 GHz. A first-order statistical analysis of the measured RCSs is firstly reported prior to assessing the radar detection performance on both measured and bespoke simulated data (leveraging the results of the developed statistical analysis), including, as benchmark terms, the curves for non-fluctuating and Rayleigh fluctuating targets.

1 Introduction

The detection of small Unmanned Aerial Vehicles (UAVs), commonly referred to as drones, is a challenging problem in both civilian and defence applications. This is due to the unsuitability of many current surveillance radars to provide adequate detection performance for such types of targets, characterized by weak radar signatures, low flight altitude and slow speed.

In this context, collecting drone data and analyzing their Radar Cross Section (RCS) is a critical step towards the design of appropriate system architectures capable of dealing with these types of targets as well as for the development of an accurate performance prediction of existing algorithms.

Not surprisingly, some valuable experimental campaigns aimed at characterizing UAV radar signatures have been conducted and the corresponding results are available in the open literature. In [1], the RCSs of small UAVs have been measured for different aspect angles in the frequency interval $8 - 12$ GHz and in VV polarization. The results have been then examined using the Inverse Synthetic Aperture Radar (ISAR) method, which provides useful information regarding the components that mostly contribute to the drone signature. The RCS measurements of two off-the-shelf drones in the frequency band $5.8 - 8.2$ GHz has been addressed in [2], and in [3] RCS data of several drones have been collected in the frequency range $26 - 40$ GHz. Some measurements in the Ku radar band have been conducted in [4], whereas, unlike aforementioned references, [5] has presented three-dimensional RCS measurements of a nano-drone from 23 GHz to 25 GHz. In [6] the RCSs of some nano and micro drones have been collected in the X-band for several elevation angles, and some statistics related to measured RCS data have been provided. Besides, [7] has presented both a statistical analysis of the measured RCS and a performance prediction of a specific UAV recognition system, whereas in [4] radar detection performance has been analyzed in the context of a short-range battlefield radar. In [8], an experimental 35 GHz Frequency-Modulated Continuous Wave (FMCW) coherent radar has been proposed to detect small UAVs, whilst [9] has investigated the detection of drones using the MIRA-CLE Ka system, which is a MIMO radar developed for imaging applications. In [10], the detection and the RCS measurement of a DJI-Phantom 4 have been assessed with the RAD-DAR, which is an experimental FMCW coherent radar operating at X-band, whereas other discussions on UAV detection via FMCW radars can be found in [11]. Furthermore, [12] has provided an overview of the state of the art in drone activity monitoring using radar systems.

To the best of the authors' knowledge, in the open literature, the assessment of radar detection performance in correspondence of bespoke target fluctuation models representing measured data in both the X and Ku radar bands has only received a limited attention. In this regard, the main scope of this paper is the evaluation of the radar performance using both measured RCSs of five drones, i.e., AscTec Firefly, AscTec Pelican, Venom VN10, Parrot AR.DRONE, and DJI Matrice 100, and tailored fluctuation models, i.e., fitting UAV RCS data. To this end, the raw RCS data are collected in a semi-controlled environment as a function of frequency, target azimuth aspect angle and polarization in the interval $8.2 - 18$ GHz. The results are analyzed considering sliding frequency intervals of 200 MHz corresponding to a range resolution of 0.75 m, which allows to model the drones as point-like targets. Furthermore, a first-order statistical analysis of the measured drones RCSs is performed by fitting the data with (one- and two- parameters) distributions typically employed to model the RCS fluctuations [13], via the minimization of the Cramér–von Mises

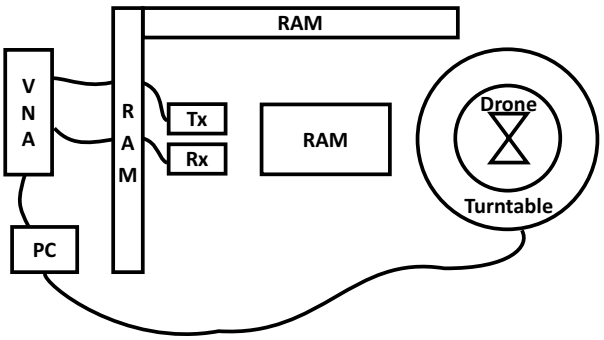

Fig. 1. A notional representation of the experimental setup.

(CVM) distance between the empirical and the theoretical Cumulative Distribution Function (CDF). Hence, in the context of a coherent detection, the radar performance is studied versus the integrated SNR at the radar receiver, with the drones RCS modeled as a fluctuating target from Coherent Processing Interval (CPI) to CPI. In particular, the detection performance, evaluated leveraging both measured and simulated fluctuations (according to the inferred distribution), is compared with standard benchmark based on stationary (Swerling 0) and random (Swerling 1) targets.

The rest of the paper is organized as follows. Section 2 presents the experimental setup and describes the pre-processing steps. The statistical behavior of the measured RCSs is analyzed in Section 3, while the radar detection performance is evaluated in Section 4. Finally, Section 5 addresses concluding remarks and outlines some possible future research avenues.

2 Experimental Setup

In this section, a description of the experimental setup involved in the measurement campaign is provided along with details on data pre-processing and calibration. The RCS data has been collected in a laboratory environment using the measurement setup depicted in Fig. 1, which is composed of

- Radar Absorbing Material (RAM) panels to mitigate multi-path reflections from the ceiling, walls and floor;
- a 2-port MS46322A Anritsu Vector Network Analyzer (VNA), which measures the frequency response of the illuminated area over a pre-defined bandwidth;
- a LinearX precision turntable with an angular step resolution of (up to) 0.1 degrees, fully controlled remotely from a PC;
- a standard PC to control and synchronize the turntable and the VNA via the Laboratory Virtual Instrument Engineering Workbench (LabVIEW) as well as to store and process the raw data;
- a pair of identical standard horn antennas, one for transmission and the other for reception; they are connected to the two ports of the VNA by means of low-loss coaxial cables and co-located on a tripod. The positions of the antennas have been adjusted with a cross-laser level to steer the antenna boresights at the target. Rotating the antennas allowed data collection for different polarizations.

Table 1 Setup and Acquisition Parameters.

Parameter	Setup 1	Setup 2
Analyzed Frequency Bandwidth	$8.2 - 12.4$ GHz	$12.4 - 18$ GHz
Azimuth Rotation Step	0.1 degrees	0.1 degrees
Target-antennas Distance	≈ 7.2 m	≈ 3.4 m
Distance from Ceiling	2.71 m	2.71 m
Height above Floor	1.28 m	1.28 m
Range Gating	$6.5 - 7.8$ m	$1.5 - 4.6$ m
Number of FFT/IFFT Points	400100	400100

Before proceeding with the measurements, the VNA has been calibrated using the standard "thru" calibration procedure to provide a measurement setup with a flat frequency response up to the antennas. The LabVIEW scripts have been designed to trigger a turntable step rotation after the data acquisition by the VNA at a specific aspect angle to guarantee collections of frequency responses with a stationary target.

Although the VNA measured all S-parameters at each frequency [14], for the considered experiments only S_{21} has been recorded and analyzed. The HH-pol and VV-pol returns from five drones have been measured versus frequency and target azimuth aspect angle in the interval $8.2 - 18$ GHz. A summary of the experimental parameters used to collect and analyze the data is reported in Table 1, whereas the specifications of the analyzed drones are listed in Table 2. Note that the employed measurement setup falls in the so-called near-field non-anechoic range scenario [15].

2.1 Data Pre-processing and Calibration

For each acquisition, a background measurement (obtained in the absence of the drone) has been collected and subtracted coherently in the frequency domain from all the data acquired in the presence of the target. Range-gating has been then applied to the high range resolution background-free profile to further isolate the target response in range from residual multi-path reflections which could not be eliminated with the Coherent Background Subtraction (CBS) [15, 16]. To achieve this, a tailored rectangular window, with parameters matched to the drone size and the target-antennas distance (see Table 1), has been used. The frequency spectrum of the clean signatures has been then used to extract the point-like target response over a moving bandwidth of 200 MHz, corresponding to a range resolution of 0.75 m. Precisely, the frequency domain is discretized in several frequency bins of 200 MHz having central frequencies $\{8.3 \text{ GHz} + (i \times 100) \text{ MHz},\ i = 0, \ldots, 96\}$ and the data are processed separately in each of them. Therein, the target can be approximated as a point-like reflector (i.e., target scatterers within the range resolution cell) whose power response (i.e., non-calibrated RCS) is extracted as the squared magnitude peak in the time domain. However, in the process of measuring the absolute RCS of a particular target, it is essential to include an accurate RCS calibration step. The substitution method [15]

Table 2 Measured Drones Specifications.

Drone	# Rotors	Weight	Width	Depth	Height	Primary Use
AscTec Firefly	6	1600 g	470 mm	430 mm	165 mm	Mapping/Surveying
AscTec Pelican	4	1650 g	360 mm	360 mm	188 mm	Film & Photo/Mapping/Surveying
Venom VN10	4	148 g	290 mm	210 mm	38 mm	Film & Photo
Parrot AR.DRONE 2.0	4	420 g	517 mm	517 mm	127 mm	Film & Photo
DJI Matrice 100	4	2355 g	759 mm	755 mm	205 mm	Film & Photo/Mapping/Surveying

is the most often used calibration procedure for RCS measurements, which involves measuring a calibrating target (with a known RCS) with the same test-bed used to collect data from the target under test [15]. As a result, each measurement related to the RCS of the calibrating target at a given frequency is compared with the theoretical RCS, and the resulting dB difference is utilized to calibrate the target measurements, provided that the test-bed, as well as the system parameters, are stationary. In the performed campaign, a conductive 10 cm diameter sphere has been used to calibrate the drone measurement data.

3 Drone RCS Statistical Behavior

The classic approach for evaluating radar detection performance is based on the assumption that the target's RCS fluctuation follows one of the Swerling models I-V [13]. However, as confirmed by some practical cases, amplitude fluctuations do not always comply with the aforementioned models, resulting in a mismatch between the actual and the theoretical radar performance. Indeed, several alternative fluctuation models (e.g., Weibull, Log-normal, shadowed Rice, two-state Rayleigh-chi, just to mention a few) have been proposed in the open literature to cope with this problem [13, 17]. Using a suitable statistical description for the target RCS behavior enables the accurate prediction of radar detection performance as well as the design of appropriate signal processing architectures. Toward this goal, in this section, the measured RCS signatures of several drones are statistically analyzed by fitting the data with well-known and commonly used distributions (at most bi-parametric), over different frequencies and polarizations. Then, the most appropriate statistical model for each drone RCS collection (in the aspect angle domain) is selected resorting to the CVM distance.

3.1 Statistical Analysis of Drones RCS

Analyzing the measured RCS of the tested drones (see Table 2), similar average RCS values are obtained in both the HH and VV polarizations, in agreement with [1]. Moreover, large fluctuations in the RCS values can be observed, which might be attributed to the presence of a few major scatterers whose interaction significantly changes with the aspect angles, with standard deviation in the order of 15 dB for the AscTec Firefly, 10 dB for the AscTec Pelican and DJI Matrice 100, and 20 dB for the Venom VN10 and the Parrot AR.DRONE 2.0.

Let us now focus on the first-order statistical analysis. Since the drones RCS strongly changes with the aspect angle, it appears reasonable the exploitation of a statistical model to describe the target fluctuation and accurately predict radar detection performance. Inspired by previous studies on target RCS fluctuation statistics, in this paper some distributions (at most bi-parametric), i.e., Exponential, Gamma, LogNormal, and Weibull, are studied to model the RCS data.

The fitting of the above-mentioned distributions with the data is performed considering the RCS measurements for different aspect angles at a given frequency f and in a polarization $p = \{HH, VV\}$. Formally, the parameter vector of the distributions is determined as a solution to the following optimization problem

$$\widehat{\boldsymbol{\theta}}(f,p) = \arg\min_{\boldsymbol{\theta}} CVM(\hat{\boldsymbol{\sigma}}(f,p), F(x;\boldsymbol{\theta})) \qquad (1)$$

where $F(x;\boldsymbol{\theta})$ is the CDF of the distribution under test, $\boldsymbol{\theta}$ denotes the distributional parameters, $\hat{\boldsymbol{\sigma}}(f,p) \in \mathbb{R}^n$, with $n = 3600$, is the vector of the measured/observed RCS, and $CVM(\hat{\boldsymbol{\sigma}}(f,p), F(x;\boldsymbol{\theta}))$ is the CVM distance [18], with $\mathbb{R}^N$ the set of N-dimensional column vectors of real numbers. The optimization problem (1) is tackled by means of the iterative algorithm proposed in [19] which is implemented in MATLAB with the function *fminsearch*, using as initial estimate of the distributional parameters those obtained via the MATLAB function *fitdist*.

Table 3 reports the mean values (over the frequency) of the CVM distances computed between the empirical and theoretical CDFs of the measured RCSs in both HH and VV polarizations. Interestingly, the Gamma model is able to achieve the lowest average CVM distance in almost all the scenarios, with some exceptions where Weibull distribution prevails over the others (see for instance the case of Asctec Pelican in HH or Venom VN10 in VV). However, under these specific instances, the mean CVM distances achieved by the Gamma and the Weibull model are relatively close. Moreover, unlike the Weibull, the Gamma fluctuation law enables a quite simple and closed-form analytical evaluation of the detection performance [17]. Furthermore, to confirm the quality of the aforementioned model to faithfully describe the collected data, a KS test is performed [18], which unveils that, regardless of the frequency and the polarization, the hypothesis that the data are distributed according to the Gamma distribution cannot be rejected.

Moreover, for almost all the cases the shape parameter α of the fitted Gamma is close to 1, underlining that the measured RCS first-order statistics are not far from an Exponential-like behavior.

Table 3 Mean CVM distances between empirical and theoretical CDF.

	mean CVM distance HH / VV				
Distribution	**AscTec Firefly**	**AscTec Pelican**	**Venom VN10**	**Parrot AR.DRONE 2.0**	**DJI Matrice 100**
Exponential	0.93 / 0.73	1.21 / 1.43	1.17 / 1.08	0.93 / 0.99	0.85 / 0.77
Gamma	**0.59 / 0.49**	0.73 / **0.66**	**0.62** / 0.69	**0.66 / 0.57**	**0.62 / 0.55**
LogNormal	1.11 / 1.37	1.09 / 1.15	1.26 / 1.32	1.06 / 1.21	0.98 / 1.04
Weibull	0.63 / 0.50	**0.67** / 0.68	0.65 / **0.66**	0.67 / 0.58	0.64 / 0.58

4 Radar Detection Performance

In this section, the radar capabilities to detect UAVs is analyzed by comparing performance under experimental target fluctuations with that resulting from appropriate statistical models. In particular, due to the huge fluctuations in RCS and hence in the resulting SNR of the received radar signal, the detection performance would also be extremely dependent on the aspect angle. Therefore, an average performance based on a statistical model for the target RCS (modeled as a random variable) is a viable mean to carry out a detection analysis [20, 21]. In this respect, it is assumed that the target's scatterers, whose composition determines the RCS value, are all within a resolution cell. The Probability of Detection ($\mathrm{P_D}$), computed assuming a desired Probability of False Alarm $P_{fa} = 10^{-4}$, is used as performance metric.

In the following, it assumed that a standard pulse-Doppler radar illuminates the target (in the Fraunhofer region) for a CPI $\tilde{T} = MT$, with M the number of pulses and T the Pulse Repetition Interval (PRI). It is assumed that the azimuth aspect angle of the drone is constant within the CPI, namely, the target amplitude does not change from pulse to pulse. Therefore, for a radar operating with a carrier frequency f and polarization $p \in \{HH, VV\}$, the received signal can be modeled as

$$\boldsymbol{r} = a(\theta, f, p)e^{j\phi}\boldsymbol{s} + \boldsymbol{n} \tag{2}$$

where

- $a(\theta, f, p)$ denotes the useful signal strength which accounts for the target RCS (at aspect angle θ) and the other terms involved in the radar equation;
- ϕ accounts for the target phase response, including the target range, and it is assumed uniformly distributed over $[0, 2\pi]$;
- $\boldsymbol{s} = [1, e^{j2\pi f_d T}, \ldots, e^{j2\pi f_d (M-1)T}]^{\mathrm{T}}$ represents the Doppler steering vector evaluated in correspondence of the Doppler frequency f_d (assumed known), with $(\cdot)^{\mathrm{T}}$ the transpose operator and $j = \sqrt{-1}$;
- $\boldsymbol{n} \sim CN(0, \sigma_n^2 \boldsymbol{I})$ is the interference plus noise contribution, modeled as a zero-mean complex circularly symmetric Gaussian random vector, with covariance matrix $\sigma_n^2 \boldsymbol{I}$; therein, σ_n^2 is the noise power level assumed, without loss of generality, equal to 0 dB.

Let us define the actual integrated SNR for the specific target aspect angle θ as $\mathrm{SNR}_c(\theta, f, p) = \overline{\mathrm{SNR}}_c \frac{\sigma(\theta,f,p)}{\tilde{\sigma}(f,p)}$, with $\overline{\mathrm{SNR}}_c$ the average integrated SNR over the aspect angle and $\tilde{\sigma}(f, p)$ the mean target RCS value. Then, the probability of detection for the optimum coherent detector at the aspect angle θ can be obtained as [13]

$$\mathrm{P_D}(\overline{\mathrm{SNR}}_c, \theta, f, p) = Q\left(\sqrt{2\overline{\mathrm{SNR}}_c \frac{\sigma(\theta, f, p)}{\tilde{\sigma}(f, p)}}, \sqrt{-2\log P_{fa}}\right), \tag{3}$$

with $Q(\cdot)$ denoting the Marcum Q function [22]. Hence, the mean detection performance over the aspect angle at given carrier frequency f and polarization p can be computed averaging (3) over all the looking angles.

To validate the fluctuation models inferred in Section 3, the resulting average $\mathrm{P_D}$ for each theoretical distribution are considered. Specifically, the $\mathrm{P_D}$ corresponding to the Gamma fluctuation model (whose closed-form expression is available in [17]) is estimated via standard Monte Carlo counting techniques over 10^4 independent trials, with the integrated SNR given by $\mathrm{SNR}_c(\theta, f, p) = \overline{\mathrm{SNR}}_c \frac{\rho(f,p)}{\mu(f,p)}$, where $\rho(f, p)$ is randomly drawn from a Gamma distribution with parameters inferred from the fitting procedure, whereas $\mu(f, p)$ denotes its corresponding expected value. Therefore, it results in an average $\mathrm{P_D}$

$$\mathrm{P_D}(\overline{\mathrm{SNR}}_c, f, p) = \frac{1}{10^4}\sum_{i=1}^{10^4} Q\left(\sqrt{2\overline{\mathrm{SNR}}_c \frac{\rho(f, p)}{\mu(f, p)}}, \sqrt{-2\log P_{fa}}\right). \tag{4}$$

For comparison purposes, the $\mathrm{P_D}$ curves $\mathrm{P_{D}}_{SW0}$ and $\mathrm{P_{D}}_{SW1}$ for non-fluctuating (SW0) and fluctuating (SW1) targets [13], respectively, are also included, where

$$\mathrm{P_{D}}_{SW0}(\overline{\mathrm{SNR}}_c) = Q\left(\sqrt{2\overline{\mathrm{SNR}}_c}, \sqrt{-2\log P_{fa}}\right) \tag{5}$$

and

$$\mathrm{P_{D}}_{SW1}(\overline{\mathrm{SNR}}_c) = P_{fa}^{1/(1+\overline{\mathrm{SNR}}_c)}. \tag{6}$$

$\mathrm{P_D}$ versus $\overline{\mathrm{SNR}}_c$ related to the AscTec Firefly is displayed in Fig. 2 for three different frequencies, i.e., 2(a) 14.1 GHz, 2(b) 8.5 GHz, and 2(c) 17.1 GHz. The values of the involved Gamma shape parameter are reported in Table 4. Specifically, Figs. 2(a) considers the scenario of Exponential-like RCS fluctuation behavior, i.e., $\alpha \approx 1$, whilst Fig. 2(b) and Fig. 2(c) refer respectively to the largest and the lowest values of the shape parameter, which are achieved, for this UAV, at the polarization HH and VV, respectively (see Table 4). The figure shows nearly perfect adherence (with negligible displacements) between the $\mathrm{P_D}$ curves obtained using measured and simulated data in all the reported cases, proving that, also from a radar detection standpoint, the fitted Gamma distribution is able to describe the measured data. Furthermore, the results outline that the $\mathrm{P_D}$

curves pertaining to the drone data are always distant from the SW0 benchmark, but quite close to those of the SW1 model. This emerging trend is expected given the observed RCS Exponential-like fluctuation characteristics highlighted in Section 3. In this regard, the results clearly pinpoint that when α is close to 1 (see Fig. 2(a)), the standard SW1 model provides accurate performance prediction. Conversely, the more the shape parameter value deviates from 1, the larger the discrepancy between the predicted performance with the SW1 model and the actual one. Unarguably, the 1.5 dB $\overline{\text{SNR}}_c$ difference at $\text{P}_\text{D} = 0.9$ between the aforementioned curves (in HH), illustrated in Figs. 2(b) and 2(c), standouts that there are specific circumstances where the performance predicted with the SW1 model leads to an inaccurate performance estimate of the radar detection task. The larger the value of α (provided that $\alpha > 1$), the larger the underestimate. In a similar manner, as α approaches 0, the overestimation increases.

Moreover, the trend of Fig. 2(a) is confirmed also for the other collected drones RCS data, i.e., the SW1 model yields an accurate performance prediction, as long as the shape parameter is close to 1. Again, particular attention should be paid to the cases where the shape parameter α of the fitted Gamma model deviates from 1. Some instances falling into this last scenario are analyzed in Fig. 3; therein (see Table 5 for the corresponding values of the Gamma shape parameter) Fig. 3(a) refers to the Venom VN10 at 9.1 GHz, Fig. 3(b) shows the Parrot AR.DRONE at 14 GHz, Fig. 3(c) considers the AscTec Pelican at 9.2 GHz. In all the examined cases, a discrepancy between the actual and the SW1 performance curves is clearly experienced in both polarizations. This behavior, previously analyzed in Figs. 2(b) and 2(c), is again reflected in the results under investigation pertaining to the other drones, which further corroborates the requirement for tailored (bi-parametric) fluctuation models to accurately predict the UAVs radar detection performance.

Table 4 Values of the Gamma shape parameter for the frequencies analyzed in Fig. 2.

Frequency	α_{HH}	α_{VV}
14.1 GHz	1.05	1.08
8.5 GHz	1.33	1.08
17.1 GHz	1.15	0.9

Table 5 Values of the Gamma shape parameter pertaining to the cases analyzed in Fig. 3.

Drone	**Frequency**	α_{HH}	α_{VV}
Venom VN10	9.1 GHz	1.57	1.08
Parrot AR.DRONE	14 GHz	0.95	1.31
AscTec Pelican	9.2 GHz	0.69	1.27

5 Conclusion

This paper has considered the radar detection performance prediction leveraging measured RCS of small UAVs collected in a semi-controlled environment as a function of frequency, angle, and polarization. Specifically, RCS measurements from five drones of different sizes and characteristics have been acquired in the frequency range 8.2-18 GHz and statistically analyzed over a moving bandwidth of 200 MHz. The results have highlighted that, in the considered frequency bands, the RCSs of the drones are characterized by strong fluctuations in angle. However, from a statistical standpoint, the Gamma distribution proved capable of modeling such measurement variability, characterized, in the majority of cases, by Exponential-like fluctuations (described using Gamma shape parameter values close to 1). The detection performance has been evaluated using both collected and simulated data (via Monte Carlo counting technique) considering as terms of comparison the standard Swerling 0 and Swerling 1 models. Usually, the curves exhibit performance deviations in the order of dB fractions from the Rayleigh fluctuating target case.

Future research avenues might consider further statistical analyses including RCS measurements collected in cross-polarization as well as the investigation of the corresponding radar detection performance by resorting to a full polarimetric processing architecture.

Acknowledgement

The work of V. Carotenuto was supported by the research program PON R&I AIM1878982-1.

References

[1] Pieraccini, M., Miccinesi, L. and Rojhani, N.: 'RCS measurements and ISAR images of small UAVs', *IEEE Aerosp Electron Syst Magazine*, 2017, **32**, (9), pp. 28–32

[2] Herschfelt, A., Birtcher, C.R., Gutierrez, R.M., Rong, Y., Yu, H., Balanis, C.A., et al.: 'Consumer-grade drone radar cross-section and micro-doppler phenomenology'. 2017 IEEE Radar Conference (RadarConf), 2017. pp. 0981–0985

[3] Semkin, V., Haarla, J., Pairon, T., Slezak, C., Rangan, S., Viikari, V., et al.: 'Analyzing radar cross section signatures of diverse drone models at mmWave frequencies', *IEEE Access*, 2020, **8**, pp. 48958–48969

[4] Ochodnický, J., Matousek, Z., Babjak, M. and Kurty, J.: 'Drone detection by Ku-band battlefield radar'. 2017 International Conference on Military Technologies (ICMT), 2017. pp. 613–616

[5] Balleri, A.: 'Measurements of the radar cross section of a nano-drone at K-band'. 2021 IEEE 8th International Workshop on Metrology for AeroSpace (MetroAeroSpace), 2021. pp. 283–287

[6] Sedivy, P. and Nemec, O.: 'Drone RCS statistical behaviour', *STO-MP-MSG-SET-183*, 2021,

[7] Ezuma, M., Anjinappa, C.K., Funderburk, M. and Guvenc, I.: 'Radar cross section based statistical recognition of UAVs at microwave frequencies', *IEEE Trans Aerosp Electron Syst*, 2022, **58**, (1), pp. 27–46

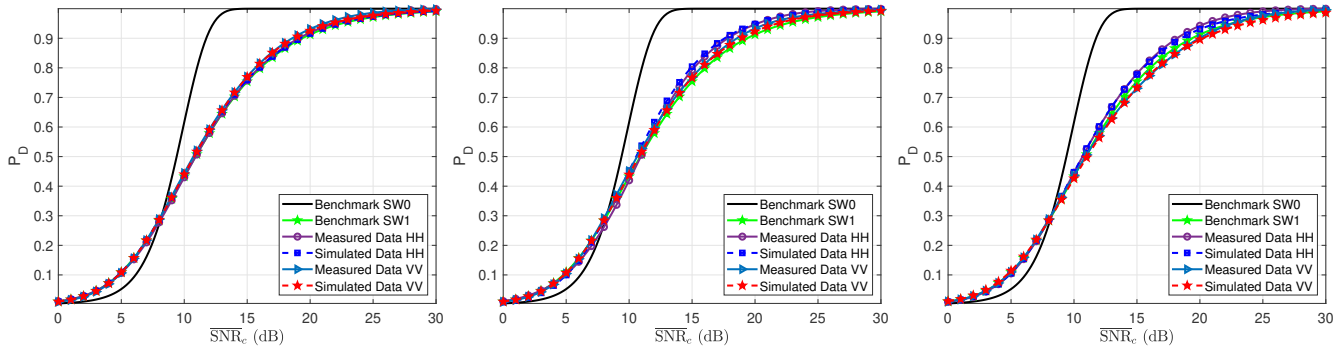

(a) (b) (c)

Fig. 2 P_D versus $\overline{SNR}_c$ curves using measured and simulated AscTec Firefly data for HH and VV polarization in the frequency bin with central frequency: (a) 14.1 GHz, (b) 8.5 GHz, and (c) 17.1 GHz.

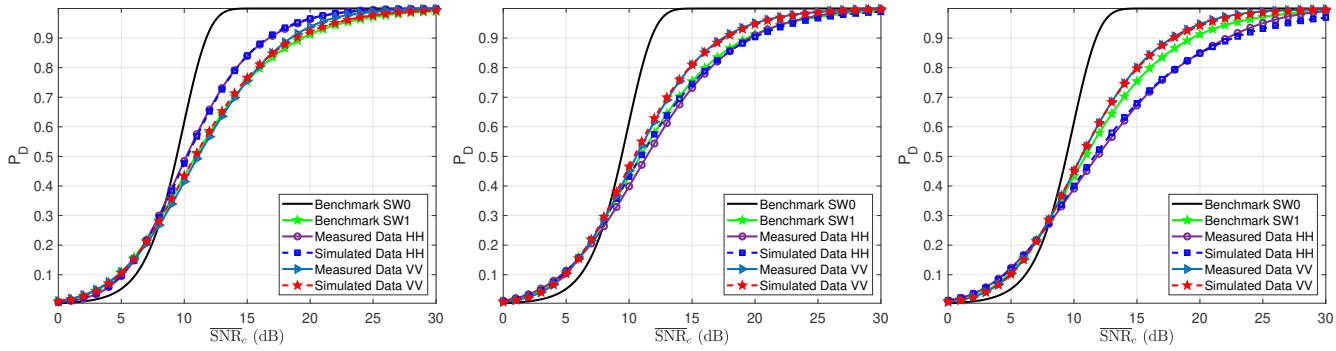

(a) (b) (c)

Fig. 3 P_D versus $\overline{SNR}_c$ for HH and VV polarization curves using measured and simulated drones data: (a) Venom VN10 at 9.1 GHz, (b) Parrot AR.DRONE at 14 GHz, (c) AscTec Pelican at 9.2 GHz.

[8] Drozdowicz, J., Wielgo, M., Samczynski, P., Kulpa, K., Krzonkalla, J., Mordzonek, M., et al.: '35 GHz FMCW drone detection system'. 2016 17th International Radar Symposium (IRS), 2016. pp. 1–4

[9] Klare, J., Biallawons, O. and Cerutti.Maori, D.: 'Detection of UAVs using the MIMO radar MIRA-CLE Ka'. Proceedings of EUSAR 2016: 11th European Conference on Synthetic Aperture Radar, 2016. pp. 1–4

[10] de Quevedo, A.D., Urzaiz, F.I., Menoyo, J.G. and López, A.A.: 'Drone detection and radar-cross-section measurements by RAD-DAR', *IET Radar, Sonar & Navigation*, 2019, **13**, (9), pp. 1437–1447

[11] Caris, M., Johannes, W., Sieger, S., Port, V. and Stanko, S.: 'Detection of small UAS with W-band radar'. 2017 18th International Radar Symposium (IRS), 2017. pp. 1–6

[12] Clemente, C., Fioranelli, F., Colone, F. and Li, G.: 'Radar Countermeasures for Unmanned Aerial Vehicles'. (London: IET, 2021)

[13] Richards, M.A., Scheer, J.A. and Holm, W.A.: 'Principles of Modern Radar: Basic Principles, Volume 1'. (Institution of Engineering and Technology, 2010)

[14] Calibration and Measurement Guide: 'Shock-Line MS46122A/B, MS46131A, ME7868A, and MS46322A/B Series Vector Network Analyzer'. 10410-00336. (Anritsu Company, 2021)

[15] IEEE: 'Recommended practice for radar cross-section test procedures', *IEEE Std 1502-2020 (Revision of IEEE Std 1502-2007)*, 2020, pp. 1–78

[16] Sundermeier, M.F. and Fischer, D.: 'Compact radar cross-section measurement setup and performance evaluation', *Advances in Radio Science*, 2021, **19**, pp. 147–152

[17] De Maio, A., Farina, A. and Foglia, G.: 'Target fluctuation models and their application to radar performance prediction', *IEE Proceedings-Radar, Sonar and Navigation*, 2004, **151**, (5), pp. 261–269

[18] D'Agostino, R. and Stephens, M.: 'Goodness-of-Fit Techniques'. (New York: Marcel Dekker, 1986)

[19] Nelder, J.A. and Mead, R.: 'A simplex method for function minimization', *The computer journal*, 1965, **7**, (4), pp. 308–313

[20] Meyer, D.P. and Mayer, H.A.: 'Radar target detection-handbook of theory and practice', *New York, Academic Press, Inc, 1973 508 p*, 1973,

[21] Swerling, P.: 'Probability of detection for fluctuating targets', *IRE Transactions on Information Theory*, 1960, **6**, (2), pp. 269–308

[22] Marcum, J.: 'A statistical theory of target detection by pulsed radar', *IRE Transactions on Information Theory*, 1960, **6**, (2), pp. 59–267